Ceramics International 46 (2020) 1220–1226

Contents lists available at ScienceDirect

Ceramics International

journal homepage: www.elsevier.com/locate/ceramint

Short communication

Enhancing the catalytic activity of recyclable nanocrystalline $NiFe_2O_4$ by replacing Ni by Cu

P.N. Anantharamaiah[a,*], Sanjukta Mondal[a], K.S. Manasa[a], Sujoy Saha[b], Maya Pai M[a]

[a] Department of Chemistry, Faculty of Mathematical and Physical Sciences, M. S. Ramaiah University of Applied Sciences, Bangalore, 560058, India
[b] Department of Materials Engineering, Indian Institute of Science, Bangalore, 560012, India

ARTICLE INFO

Keywords:
Nickel ferrite
Cu-substitution
Catalytic reduction
Crystallite size
4-Nitrophenol

ABSTRACT

Herein, we report an efficient, magnetically recoverable and recyclable nanocatalyst to drive a reduction reaction under mild reaction conditions. Nickel ferrite ($NiFe_2O_4$) and 20% copper substituted nickel ferrite ($Ni_{0.8}Cu_{0.2}Fe_2O_4$) nanocatalysts were synthesized using a facile glycine-nitrate autocombustion route and employed as catalysts to assess the reduction of 4-nitrophenol in aqueous medium. Phase purity, structural aspects, morphological features and magnetic characteristics of as-synthesized ferrite powders were carried out using X-ray diffraction (XRD), transmission electron microscopy (TEM) and vibrating sample magnetometer (VSM). **Elemental compositions of the prepared materials were investigated using EDX analysis**. Reduction of 4-nitrophenol to 4-aminophenol using $NaBH_4$ as the reducing agent with the nanocatalyst was monitered using a UV–Visible spectrophotometry. The results indicate that the $Ni_{0.8}Cu_{0.2}Fe_2O_4$ demonstrated a better catalytic activity with nearly 99% conversion against $NiFe_2O_4$, which showed almost negligible activity over a long period of time. For the first catalytic reduction cycle, time taken by the $Ni_{0.8}Cu_{0.2}Fe_2O_4$ was less than 2 min. However, the reduction time increased progressively as number of cycles increased. $Ni_{0.8}Cu_{0.2}Fe_2O_4$ also displayed a superior catalytic performance over 10 cycles, without a significant drop in its activity. The superior catalytic performance of $Ni_{0.8}Cu_{0.2}Fe_2O_4$ is likely to be due the surface contribution of smaller particles and the presence of Cu^{2+} at the octahedral site of the spinel ferrite.

1. Introduction

Among the aromatic pollutants, nitrophenol and its derivatives are considered as the most common organic pollutants in agricultural and industrial waste water [1,2]. Conversely, aminophenol and its derivatives are of great economical importance as they are the starting materials or intermediates to design numerous products such as drugs, dyestuffs, rubber chemicals, etc [3,4]. Therefore, it is imperative to convert nitrophenols to aminophenols in an economical way. In this direction, constant research efforts are in progress to develop a most capable catalyst for the conversion from the toxic nitrophenols to value added aminophenols under mild reaction conditions. So far, wide range of catalysts such as metal oxides [5], highly expensive metal nanoparticles such as Pd, Ag, Au, Pt [6–9] and composite materials [10,11] have been developed for the reduction or degradation of nitrophenols. In recent times, magnetic nanomaterials, particularly spinel-type ferrite systems, are being studied as suitable alternative catalysts to drive the reduction of 4-nitrophenol to 4-aminophenol in aqueous medium [12–15]. The spinel ferrites are soft magnetic in nature, and thus they could be selectively separated from a complex heterogeneous mixture by an external magnetic field. Apart from this, the nano-sized spinel ferrites are chemically stable, causy to prepare in large scale, non-toxic in nature and more importantly cost-effective, and hence they are the suitable candidates [15]. The catalytic performance associated with the spinel ferrites is governed by several factors such as cation distribution, surface area, morphological features and particle size distribution. Moreover these factors indeed depend on synthesis methods and processing conditions [15].

Singh et al. [15] employed nanocrystalline $CoFe_{2-x}Ni_xO_4$ ($0 \leq x \leq 1$), synthesized using the reverse micelle technique, as catalysts for reduction of 4-nitrophenol using $NaBH_4$ as the reducing agent, and reported increased catalytic activity as Ni content increased in the $CoFe_2O_4$ lattice. Feng et al. [13] have synthesized copper ferrite nanoparticles and employed as catalyst for the reduction of 4-nitrophenol in the presence of $NaBH_4$ as reducing agent, and showed $>$ 95% conversion in $<$ 40 s. But the authors have discovered Cu metal phase together with the copper ferrite phase in the XRD pattern, and the role of Cu phase on the catalytic reduction of 4-nitrophenol had not been

* Corresponding author.
E-mail address: anantharamaiah.cy.mp@msruas.ac.in (P.N. Anantharamaiah).

https://doi.org/10.1016/j.ceramint.2019.08.276
Received 23 March 2019; Received in revised form 28 August 2019; Accepted 30 August 2019
Available online 30 August 2019

discussed. Rath et al. [16] have showed in their report that nano-sized Cu, Cu_2O and CuO impreganted on cubic order mesoporous carbon would also serve as effective catalysts for the reduction of 4-nitrophenol to 4-aminophenol. Goyal et al. [12] investigated the catalytic efficiency of nano-sized MFe_2O_4 (M = Zn, Cu, Ni), synthesized using the sol-gel route, for the reduction of nitrophenols in the presence of $NaBH_4$, and reported better activity for $CuFe_2O_4$ against other two ferrites. Even in this report, the authors have noticed CuO as secondary phase along with prominent $CuFe_2O_4$ phase and no discussion was made on the contribution of CuO towards the nitrophenol reduction properties. In most of the reports on the spinel-type ferrites as catalysts, reusablibilty of the nano ferrite catalysts for multiple cycles and phase stability of the catalyts after the application were not explored. Therefore, it is indispensable to synthesize high-performance single phase nanocrystalline ferrites and exploit them as catalysts for the reduction of 4-nitrophenol and also for multiple cycles.

In this study, single phase nanocrystalline $NiFe_2O_4$ and $Ni_{0.8}Cu_{0.2}Fe_2O_4$ compositions have been synthesized and employed as catalysts for reduction of 4-nitrophenol in the presence of the $NaBH_4$. After introduction of Cu into the $NiFe_2O_4$ lattice, a remarkable enhancement in the catalytic performance has been observed under mild reaction conditions. Furthermore, $Ni_{0.8}Cu_{0.2}Fe_2O_4$ demostarted better performance for more than 10 cycles, without a significant drop in its activity.

2. Experimental

2.1. Synthesis of ferrite nanocatalysts

$Ni(NO_3)_2$ $6H_2O$, $Cu(NO_3)_2$ $6H_2O$, $Fe(NO_3)_3$ $9H_2O$, glycine, and 4-nitrophenol were procured from Merck (India) chemicals and used without further purification. $NiFe_2O_4$ (NFO) and $Ni_{0.8}Cu_{0.2}Fe_2O_4$ (NC2FO) were synthesized by following the glycine-nitrate auto-combustion method [17]. Initially, metal nitrates were weighed accurately according to stoichiometric ratios for each composition and dissolved in minimum amounts of distilled water followed by 10 min sonication. To the metal nitrates solution, a solution of glycine (0.5 mol per mole of metal ion) was added and sonicated for 15 min to achieve a homogeneous reaction mixture. Subsequently, the reaction mixture was placed on a hot plate at 200 °C. A thick viscous gel was formed after the solvent evoporated, which underwent instantaneous combustion yeilding the corresponding ferrite powders.

2.2. Materials characterization

Phase purity and average crystallite sizes of the as-synthesized ferrite powders were ascertained using a powder X-ray diffractometer (Rigadu, Smart Lab) using monochromatic CuKα (λ = 1.5406 Å) radiation. Morphology and particle size of the ferrite powders were assessed using a transmission electron microscope (Tecnai G2 F30). **Elemental mapping and EDX analyses were performed with a scanning electron microscopy equipped with UltraDry EDS detector (ESEM EFI Quanta 200). Raman spectra were recorded at room temperature using a micro-Raman spectrometer (Horiba JY LabRam HR 800) using 532 nm.** Magnetic measurements were carried out at room temperature using an EG&G PAR 4500 vibrating sample magnetometer. Time dependent UV–Visible spectra were recorded at room temperature using a UV–visible spectrophotometer (Shimadzu UV-2600).

2.3. Catalytic reduction of 4-nitrophenol

The catalytic reduction of 4-nitrophenol to 4-aminophenol was employed as a model reaction to assess the performance of NFO and NC2FO as catalysts. At the beginning, freshly prepared 0.2 M aqueous solution of $NaBH_4$ was added to a 50 ml of 0.02 mM aquesous solution of 4-nitrophenol, and the reaction mixture was subjected to constant stirring at ambient temperature. Soon after the addition of $NaBH_4$, the colour of the 4-nitrophenol solution instantly transformed from pale yellow to intense yellow, due to the production of phenolate anion. Afterwards, 15 mg of the ferrite nanocatalyst was added to the reaction mixture and stirring was continued under the same conditions. It was noticed that the intensity of the yellow colour faded gradually with time, revealing the catalytic reduction of 4-nitrophenol. Progress of the reaction was tested by recording UV–visible absorption spectra in the range of 200–600 nm of small portions (~3 ml) of the reaction mixture extracted at different time intervals. Decreasing the intensity of the absorption band at 400 nm due to the phenolate anion and emergence of a new band at 303 nm indicated the formation of 4-aminophenol.

2.4. Recovery and reusability of the catalyst

After completion of the reduction reaction, the catalyst was magnetically recovered using a laboratory magnet of strength 0.2 T and washed with distilled water for several times. The reduction reaction was repeated several times using the recovered catalyst from the previous reaction. After eleven cycles, the recovered catalyst was washed with distilled water and subsequently dried at 70 °C in an oven. The dried recovered catalyst was investigated by XRD to assess the phase stability.

3. Results and discussion

3.1. X-ray diffraction (XRD), transmission electron microscopy (TEM) and scanning electron microscopy (SEM) mapping

Fig. 1(a) shows the powder XRD patterns of the as-synthesized NFO and NC2FO compared with the simulated pattern of $NiFe_2O_4$, generated using the powder cell for windows (PCW) [18]. All the reflections in the XRD patterns of both the as-synthesized compositions match with that in the simulated pattern, suggesting formation of single phase cubic spinel-type ferrites. Moreover, the peaks in the experimental patterns are broad, signifying nanocrystalline nature of the particles. Using the Scherrer formula [19], the average crystallite sizes of the compositions are calculated from the width of the most intense (311) peak, after subtracting the instrumental contribution to the peak broadening. The average crystallite sizes are obtained 17 nm and 12 nm, respectively, for NFO and NC2FO. The samller crystallite size obtained for NC2FO against the NFO is most probably due to the induced lattice strain, due to the slightly larger size of Cu^{2+} compared to Ni^{2+}, as suggested in the earlier reports [19]. Using the Williamson-Hall analysis [20], the lattice strain of the compositions was estimated and the values are summerized in Table 1. Even after replacing 20% Ni^{2+} by Cu^{2+} in the lattice of spinel ferrite, the cubic lattice parameter, calculated by least-squares fitting of the experimental pattern, was found to be nearly the same for both NFO and NC2FO (see Table 1) due to comparable ionic radii of Cu^{2+} and Ni^{2+}, and possible re-distribution of the different ions in the tetrahedral and octahedral sites of the spinel lattice. The ionic radii of Ni^{2+} and Cu^{2+} are 0.55 and 0.57 Å for tetrahedral coordination and 0.69 and 0.73 Å for octahedral coordination [21].

The morphological features and particle sizes of the as-sythesized NFO and NC2FO powders were further evaluated by TEM. TEM images of NFO and NC2FO are presented in Fig. 1(b) and (c). It is apparent from the TEM images that the particles are nearly spherical in morphology with approximately narrow size distribution. Furthermore, the particles of NC2FO are smaller in size in comparison with that of NFO, **as illustrated by the histograms of particle size distribution in** Fig. 1. The average particle size, measured from the TEM images, is nearly comparable with the average crystallite size calculated from the XRD patterns (See Table 1).

Images of elemental mapping and energy dispersive X-ray analysis (EDX) spectrum of the nanocrystalline NC2FO sample are presented in

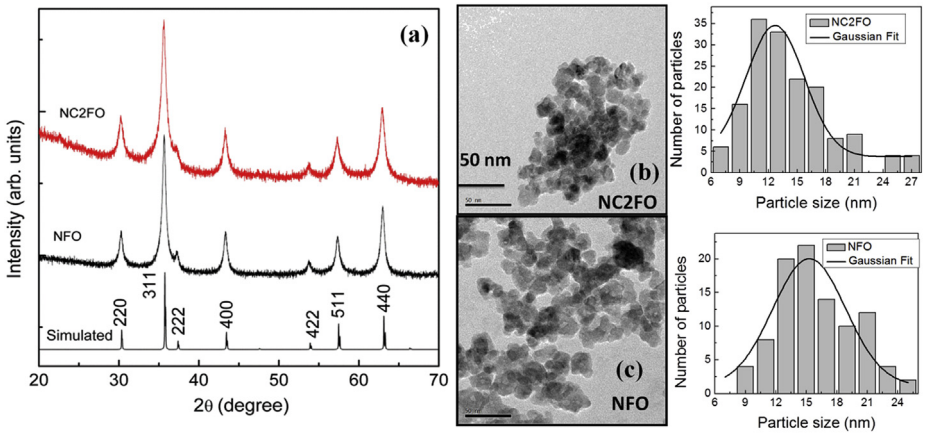

Fig. 1. (a) XRD patterns of the as-synthesized NFO ($NiFe_2O_4$) and NC2FO ($Ni_{0.8}Cu_{0.2}Fe_2O_4$) samples compared with the simulated XRD pattern of $NiFe_2O_4$.(b) and (c) are TEM images of NC2FO and NFO, respectively. Histograms of particle size distribution of the corresponding samples are also presented.

Fig. 2. As can be seen from the mapping images, the elements such as iron (Fe), nickel (Ni) and copper (Cu) are present in the sample, and moreover the elements are uniformly dispersed. From the EDX analysis, the elemental compositions of the samples were estimated and the results are presented in Table 2. The elemental compositions of the samples, estimated from the EDX analysis, are nearly comparable with the targeted compositions.

3.2. Raman spectra

According to the factor group analysis, compounds with normal spinel structure are expected to exhibit merely five Raman active bands ($A_{1g} + E_g + 3T_{2g}$) but more than five active bands have been documented for the inverse and mixed spinels due to the cations disorder [19]. In the present study, all the characteristic Raman active bands, corresponding to the spinel structure, were observed in the Raman spectra of NFO and NC2FO, as shown in Fig. 3(a). The $A_{1g}(1)$ and $A_{1g}(2)$ pertain to symmetric breathing modes of FeO_4 and NiO_4 tetrahedral units, respectively [22]. E_g and $T_{2g}(3)$ are due to symmetric and asymmetric bending motion of oxygen coordinated to Fe and/or Ni in the tetrahedral environment, respectively. $T_{2g}(2)$ is due to symmetric stretching of FeO_6 or NiO_6 octahedral units [19,22], $T_{2g}(1)$ is due to translational movement of the whole tetrahedron [22]. It has been observed from the Raman spectra that active bands are wider and their positions are shifted towards higher wavenumbers, after incorporation of Cu^{2+} into the lattice of $NiFe_2O_4$. The more broadening and shift in the band positions could be due to the lattice strain induced in the material as a result of Cu^{2+} introduction.

To extract further information, the Raman spectra of NFO and NC2FO samples were deconvoluted and results of the deconvoluted spectra are presented in Fig. 3(b)&(c). For the unsubstituted NFO sample, the ratio of the area under the peaks due to $A_{1g}(2)$ (NiO_4) and $A_{1g}(1)$ (FeO_4) is obtained as 0.18 from which the cations distribution can be obtained as $(Ni_{0.18}Fe_{0.82})_A[Ni_{0.82}Fe_{1.18}]_BO_4$. In case of NC2FO sample, the ratio of the area under the peaks due to $A_{1g}(2)$ (NiO_4) and $A_{1g}(1)$ (FeO_4) is obtained as 0.32, indicating more Ni^{2+} ions have been replaced from the octahedral sites to the tetrahedral sites, due to substitution of Cu^{2+} at the octahedral sites.

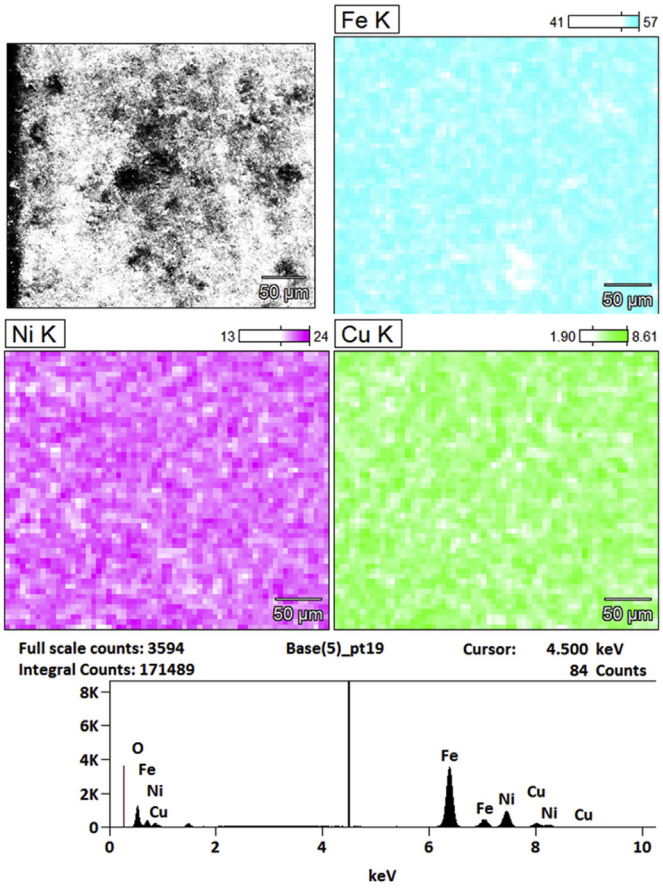

Fig. 2. Elemental mapping images of NC2FO ($Ni_{0.8}Cu_{0.2}Fe_2O_4$) sample and the corresponding energy-dispersive x-ray analysis (EDX) spectrum.

Table 1
Sample code, crystallite/particle size obtained from XRD and TEM, strain, lattice parameter (a), saturation magnetization (M_s) and coercivity (H_c) of as-synthesized NFO ($NiFe_2O_4$) and NC2FO ($Ni_{0.8}Cu_{0.2}Fe_2O_4$) samples.

Composition	Sample code	't_{XRD}' (nm)	't_{TEM}' (nm)	Strain (%)	'a' (Å)	Ms (emu/g)	Hc (kA/m)
$NiFe_2O_4$	NFO	17	16	0.0014	8.348	26	7.4
$Ni_{0.2}Cu_{0.2}Fe_2O_4$	NC2FO	12	13	0.0036	8.347	16	13.3

Table 2
Target chemical composition of $NiFe_2O_4$ (NFO) and $Ni_{0.8}Cu_{0.2}Fe_2O_4$ (NC2FO) and the final composition estimated by EDX in a SEM.

Target composition	Final composition by EDX		
	Ni	Fe	Cu
$NiFe_2O_4$	0.94	2.06	–
$Ni_{0.8}Cu_{0.2}Fe_2O_4$	0.76	2.05	0.19

3.3. Magnetic measurements

Fig. 4 illustrates the field dependence of the magnetization for the as-synthesized NFO and NC2FO compositions, recorded at ambient temperature. As evident from the inset of Fig. 4, both compositions exhibit magnetic hysteresis loops due to their ferrimagnetic nature and their magnetization is not saturated even at the maximum measuring field strength of 1.5 T (1 T = 800 kA/m). Saturation magnetization (M_s) of the compositions is obtained by extrapolating M *versus* 1/H curve to 1/H = 0 and the values are tabulated in Table 1. The M_s of NFO (26 emu/g) obtained in the present study is comparable with the values reported for the nanocrystalline nickel ferrites of similar particle sizes [23] but significantly lower than the values reported for the bulk nickel ferrite [24]. This is due to the contribution of surface spin disorder associated with the surface of the nanoparticles. After replacing 20% Ni^{2+} by Cu^{2+} in the spinel ferrite, the M_s is found to be decreased to 16 emu/g. The decrease in M_s is primarily attributed to two factors, firstly, the smaller particle size of NC2FO, and secondly, the reduced number of spins in Cu^{2+} compared to that in Ni^{2+} in the octahedral sites of the spinel ferrite [25].

The coercivity H_c of NC2FO is considerably higher than that of the unsubstituted counterpart (Table 1). The increase in the coercivity could be due to the changes in the A-O-B superexchange interactions, when Ni^{2+} (d^8, S = 1) is replaced by Cu^{2+} (d^9, S = 1/2) in the AB_2O_4 spinel structure, as well as the relatively smaller particle size.

3.4. Catalytic reduction of 4-nitrophenol

The catalytic reduction of 4-nitrophenol to 4-aminophenol was monitored by recording the absorption spectra. The changes in the intensities of the absorption bands at 400 and 303 nm, respectively, for the reactant and the product were monitored as a function of time. Even though $NaBH_4$ is a well-known for its reducing agent, it is incapable of converting 4-nitrophenol to 4-aminophenol due to the high kinetic energy barrier between the phenolate anion and BH_4^- [16]. In such a scenario, a catalyst may help to minimize the barrier of energy and thereby facilitates the reduction reaction. Here in this study, when nickel ferrite (NFO) was exploited as a catalyst to drive the reduction process, a slight drop in the intensity of the absorption peak at 400 nm due to phenolate anion, without any prominent signature of the absorption peak at 303 nm due to the 4-aminophenol, has been observed after 60 min (Fig. 5(a)), suggesting an almost insignificant reduction reaction. The time dependent UV–visible spectra using NC2FO as the catalyst demonstrated a rapid drop in the intensity of the absorption peak of the phenolate anion at 400 nm, with a simultaneous increase in the intensity of the absorption peak of the 4-aminophenol at 303 nm, as shown in Fig. 5(b). With the addition of NC2FO, the intense yellow colour of the phenolate anion solution was vanished within 2 min (see the inset of Fig. 4), revealing that the reduction reaction was very fast.

It is reported in the literature that if a substituent occupies the octahedral sites of the spinel ferrite lattice, then the catalytic activity of the metal ion-substituted spinel ferrite would be enhanced by many folds as the octahedral sites are exposed on the surface [12,15]. Thus, the metal ions located at the octahedral sites facilitate rapid transfer of electrons from borohydride (BH_4^-) to 4-nitrophenol, which leads to the formation of 4-aminophenol [15]. In the present case, remarkable enhancement of the catalytic performance after introduction of Cu^{2+} into the lattice of nickel ferrite could be due to its octahedral site preference [25]. In fact, the presence of Cu^{2+} in the octahedral site of the NC2FO is strongly supported by the magnetic and Raman data.

The UV–Visible spectra in the eleventh recycle test using NC2FO is presented in Fig. 5(c). Similar to the use of the fresh catalyst, the intensity of the absorbance band at 400 nm decreased progressively with simultaneous increase in the intensity of the band at 303 nm, as a function of time, indicating the formation of the corresponding product. However, the complete transformation of 4-nitrophenol to 4-aminophenol was achieved after 7 min, slightly higher than the period required for the fresh catalyst. The increase in the time for the reduction reaction with increasing number of cycles is most probably due to the decrease in the number of active sites decorated on the surface of the nanoparticles. Since the concentration of $NaBH_4$ is high, the reduction reaction can be assumed to obey pseudo-first order kinetics. Pseudo-first order rate constant can be estimated using the rate law equation [15].

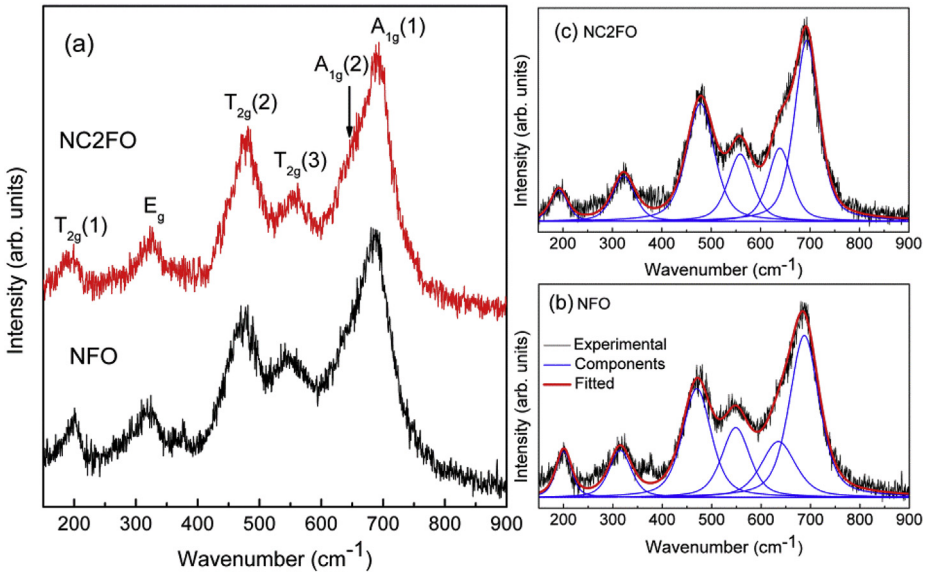

Fig. 3. (a) Raman spectra of as-synthesized NFO and NC2FO samples, recorded at room temperature, (b) and (c) are the corresponding deconvoluted spectra.

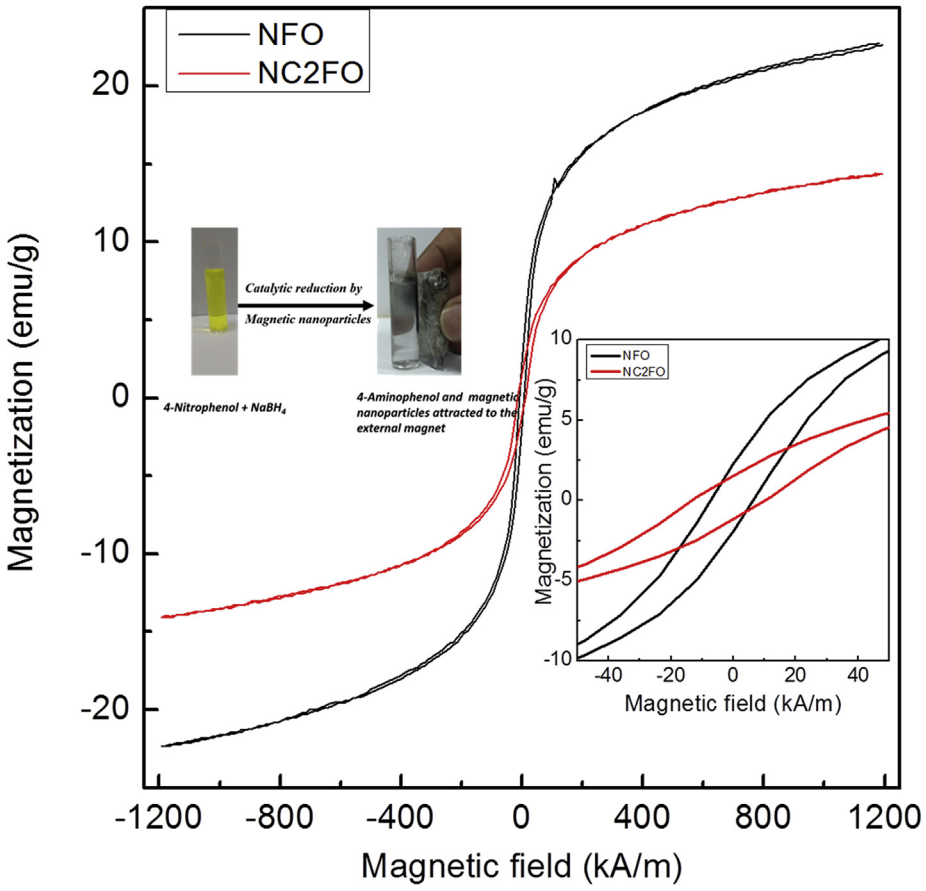

Fig. 4. M − H hysteresis loops of as-synthesized NFO ($NiFe_2O_4$) and NC2FO ($Ni_{0.8}Cu_{0.2}Fe_2O_4$) samples. Inset shows the enlarged hysteresis loops in the low field regions and the image demonstrates the magnetically separable ferrite nanocatalyst, after the reduction reaction.

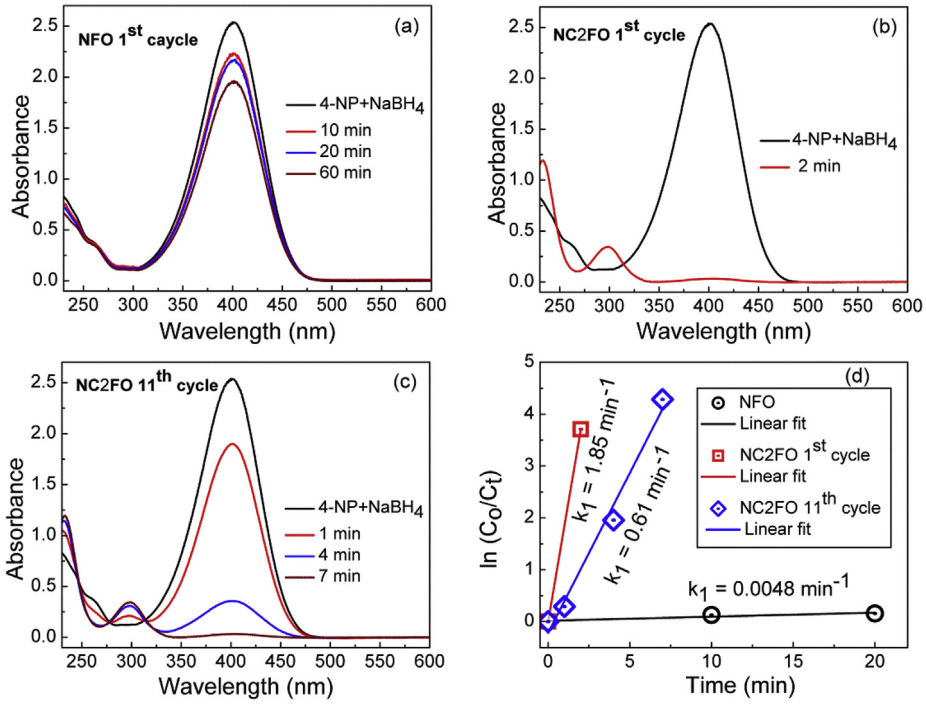

Fig. 5. UV–Visible spectra of 4-nitrophenol at different time intervals using (a) NFO, (b) 1st cycle using NC2FO, and (c) 11th cycle using NC2FO. The corresponding plots of $\ln(C_o/C_t)$ *vs* time are shown in (d).

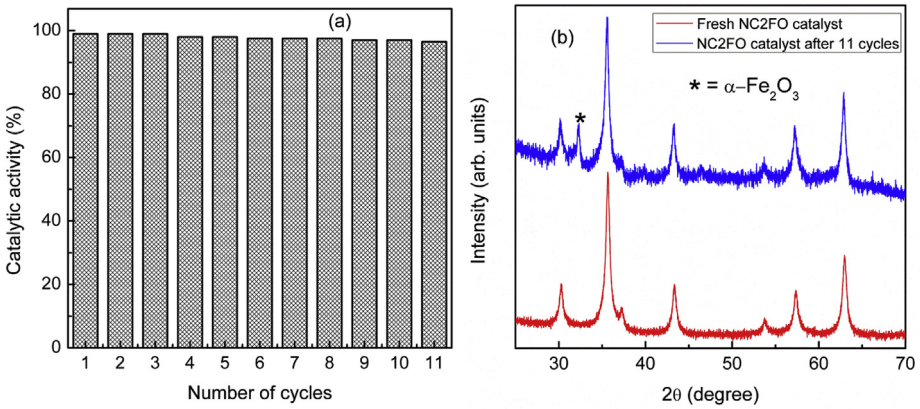

Fig. 6. (a) Reusability of NC2FO as catalyst for the reduction of 4-nitrophenol in the presence of $NaBH_4$. (b) Comparison of the powder XRD patterns of fresh and spent catalyst of NC2FO, wherein the impurity phase is represented by '*' symbol.

$$\ln\left(\frac{C_O}{C_t}\right) = -k_1 t$$

where, C_t and C_o are the concentrations at time 't' and t = 0, respectively, and k_1 is the pseudo-first order rate constant. The plot of $\ln(C_o/C_t)$ *versus* time (t) for the reduction of 4-nitrophenol in the presence of $NaBH_4$ with the catalysts (NFO and NC2FO (1st and 11th cycle tests)) is shown in Fig. 5(d). The rate constant values were estimated from the slope of the straight line obtained from the plot of $\ln(C_o/C_t)$ *versus* time (t). The rate constant values using fresh NFO, fresh NC2FO, and 11th cycle using NC2FO are obtained as 0.0048, 1.85 and 0.61 min^{-1}, respectively. Despite the fact that the time for the reduction reaction increased with number of cycles, the catalytic activity of NC2FO catalyst remains almost constant up to the 11 cycles, as shown in Fig. 6(a).

Fig. 6(b) compares the XRD patterns of the spent NC2FO catalyst recovered after the 11th cycle with that of the fresh catalyst. The XRD pattern of the spent NC2FO catalyst showed the signature of an extra peak at the diffraction angle 2θ ~33.3° and this corresponds to the phase α-Fe_2O_3. Formation of the impurity phase together with decrease in the number of active sites on the surface of the nanoparticles is most likely to be responsible for the increase in the duration of the reduction reaction with the increasing number of cycles using the recovered catalyst.

4. Conclusions

Between the nanoparticles of $NiFe_2O_4$ (NFO) and $Ni_{0.8}Cu_{0.2}Fe_2O_4$ (NC2FO), NC2FO displayed a significant catalytic performance for the reduction of 4-nitrophenol to 4-aminophenol. **The presence of Cu^{2+} at the octahedral sites of the spinel ferrite and the smaller particle size are likely to be responsible for higher catalytic activity associated with NC2FO. Magnetic and Raman data support the presence of Cu^{2+} at the octahedral sites of the spinel ferrite.** The catalytic activity remains intact with the NC2FO even after 11th cycles, except for an increase in the time required for the reduction reaction. The formation of an impurity phase, as revealed from the XRD pattern of the spent catalyst, and the decrease in the number of active sites on the surface of the nanoparticles could be accountable for the increase in the reaction time with increasing number cycles.

Acknowledgements

P. N. Anantharamaiah is grateful to Dr. P. A. Joy, CSIR-National Chemical Laboratory, Pune, for the VSM measurements. Sujoy Saha gratefully ackowledges D. S. Kothari Postdoctoral Fellowship. U.G.C, New Delhi.

References

[1] M. Zarejousheghani, M. Moder, H. Borsdorf, A new strategy for synthesis of an in-tube molecularly imprinted polymer-solid phase microextraction device: selective offline extraction of 4-nitrophenol as an example of priority pollutants from environmental water samples, Anal. Chim. Acta 798 (2013) 48–55.
[2] Y. Li, Y. Cao, J. Xie, D. Jia, H. Qin, Z. Liang, Facile solid-state synthesis of Ag/graphene oxide nanocomposites as highly active and stable catalyst for the reduction of 4-nitrophenol, Catal. Commun. 58 (2015) 21–25.
[3] M.J. Vaidya, S.M. Kulkarni, R.V. Chaudhari, Synthesis of p-aminophenol by catalytic hydrogenation of p-nitrophenol, Org. Process Res. Dev. 7 (2003) 202–208.
[4] H. Filik, G. Cetintas, S.N. Koc, H. Gulce, I. Boz, Nafion-graphene composite film modified glassy carbon electrode for voltammetric determination of p-aminophenol, Russ. J. Electrochem. 50 (2014) 243–252.
[5] G. Wu, X. Liang, L. Zhang, Z. Tang, M. Al-Mamun, H. Zhao, X. Su, Fabrication of highly stable metal oxide hollow nanospheres and their catalytic activity toward 4-nitrophenol reduction, ACS Appl. Mater. Interfaces 9 (2017) 18207–18214.
[6] Y.C. Chang, D.W. Chen, Catalytic reduction of 4-nitrophenol by magnetically recoverable Au nanocatalyst, J. Hazard Mater. 165 (2009) 664–669.
[7] L. Ai, J. Jiang, Catalytic reduction of 4-nitrophenol by silver nanoparticles stabilized on environmentally benign macroscopic biopolymer hydrogel, Bioresour. Technol. 132 (2013) 374–377.
[8] X. Lin, M. Wu, D. Wu, S. Kuga, T. Endo, Y. Huang, Platinum nanoparticles using wood nanomaterials: eco-friendly synthesis, shape control and catalytic activity for p-nitrophenol reduction, Green Chem. 13 (2011) 283–287.
[9] Z. Dong, X. Le, Y. Liu, C. Dong, J. Ma, Metal organic framework derived magnetic porous carbon composites supported gold and palladium nanoparticles as highly efficient and recyclable catalysts for reduction of 4-nitrophenol and hydrodechlorination of 4-chlorophenol, J. Mater. Chem. 2 (2014) 18775–18785.
[10] M. Ma, Y. Yang, W. Li, R. Feng, Z. Li, P. Lyu, Y. Ma, Gold nanoparticles supported by amino groups on the surface of magnetite microspheres for the catalytic reduction of 4-nitrophenol, J. Mater. Sci. 54 (2019) 323–334.
[11] O.A. Zelekewa, D.H. Kuo, Synthesis of a hierarchical structured NiO/NiS composite catalyst for reduction of 4-nitrophenol and organic dyes, RSC Adv. 7 (2017) 4353–4362.
[12] A. Goyal, S. Bansal, S. Singhal, Facile reduction of nitrophenols: comparative catalytic efficiency of MFe_2O_4 (M = Ni, Cu, Zn) nanoferrites, Int. J. Hydrogen Energy 39 (2014) 4895–4908.
[13] J. Feng, L. Su, Y. Ma, C. Ren, Q. Guo, X. Chen, $CuFe_2O_4$ magnetic nanoparticles: a simple and efficient catalyst for the reduction of nitrophenol, Chem. Eng. J. 221 (2013) 16–24.
[14] Z. Naghshbandi, N. Arsalani, M.S. Zakerhamidi, K.E. Geckeler, A novel synthesis of magnetic and photoluminescent graphene quantum dots/MFe_2O_4 (M = Ni, Co) nanocomposites for catalytic application, Appl. Surf. Sci. 443 (2018) 484–491.
[15] C. Singh, A. Goyal, S. Singhal, Nickel-doped cobalt ferrite nanoparticles: efficient catalysts for the reduction of nitroaromatic compounds and photo-oxidative degradation of toxic dyes, Nanoscale 6 (2014) 7959–7970.
[16] P.C. Rath, D. Saikia, M. Mishra, H.M. Kao, Exceptional catalytic performance of ultrafine Cu_2O nanoparticles confined in cubic mesoporous carbon for 4-nitrophenol reduction, Appl. Surf. Sci. 427 (2018) 1217–1226.
[17] K.K. Mohaideen, P.A. Joy, High magnetostriction and coupling coefficient for sintered cobalt ferrite derived from superparamagnetic nanoparticles, Appl. Phys. Lett. 101 (2012) 072405.
[18] W. Kraus, G. Nolze, Powder cell - a program for the representation and manipulation of crystal structures and calculation of the resulting X-ray powder patterns, J. Appl. Crystallogr. 29 (1996) 301–303.
[19] P.N. Anantharamaiah, P.A. Joy, Enhancing the strain sensitivity of $CoFe_2O_4$ at low magnetic fields without affecting the magnetostriction coefficient by substitution of small amounts of Mg for Fe, Phys. Chem. Chem. Phys. 18 (2016) 10516–10527.
[20] G.K. Williamson, W.H. Hall, X-ray line broadening from filed aluminium and wolfram, Acta Metall. 1 (1953) 22–31.

[21] R.D. Shannon, Revised effective ionic radii and systematic studies of interatomic distances in halides and chalcogenides, Acta Crystallogr. A 32 (1976) 751–767.
[22] Z.Ž. Lazarević1, Č. Jovalekić, A. Milutinović, D. Sekulić, V.N. Ivanovski, A. Rečnik, B. Cekić, N.Ž. Romčević, Nanodimensional spinel $NiFe_2O_4$ and $ZnFe_2O_4$ ferrites prepared by soft mechanochemical synthesis, J. Appl. Phys. 113 (2013) 187221.
[23] M. Salavati-Niasari, F. Davar, T. Mahmoudi, A simple route to synthesize nanocrystalline nickel ferrite ($NiFe_2O_4$) in the presence of octanoic acid as a surfactant, Polyhedron 28 (2009) 1455–1458.
[24] S.E. Shirsath, B.G. Toksah, K.M. Jadhav, Structural and magnetic properties of In^{3+} substituted $NiFe_2O_4$, Mater. Chem. Phys. 117 (2009) 163–169.
[25] A. Samavati, M.K. Mustafa, A.F. Ismail, M.H.D. Othman, M.A. Rahman, Copper-substituted cobalt ferrite nanoparticles: structural, optical and antibacterial properties, Mater. Express 6 (2016) 473–483.